

How do ultra-low frequency waves access the inner magnetosphere during geomagnetic storms?

Article

Accepted Version

Rae, I. J., Murphy, K. R., Watt, C. E. J., Sandhu, J. K., Georgiou, M., Degeling, A. W., Forsyth, C., Bentley, S. N., Staples, F. A. and Shi, Q. (2019) How do ultra-low frequency waves access the inner magnetosphere during geomagnetic storms? *Geophysical Research Letters*, 46 (19). pp. 10699-10709. ISSN 0094-8276 doi: 10.1029/2019GL082395
Available at <https://centaur.reading.ac.uk/83939/>

It is advisable to refer to the publisher's version if you intend to cite from the work. See [Guidance on citing](#).

To link to this article DOI: <http://dx.doi.org/10.1029/2019GL082395>

Publisher: American Geophysical Union

All outputs in CentAUR are protected by Intellectual Property Rights law, including copyright law. Copyright and IPR is retained by the creators or other copyright holders. Terms and conditions for use of this material are defined in the [End User Agreement](#).

www.reading.ac.uk/centaur

CentAUR

Central Archive at the University of Reading

Reading's research outputs online

How do Ultra-Low Frequency waves access the inner magnetosphere during geomagnetic storms?

I. Jonathan Rae,¹ Kyle R. Murphy,² Clare E. J. Watt,³ Jasmine K. Sandhu,¹ Marina Georgiou,¹ Alex W. Degeling,⁴ Colin Forsyth,¹ Sarah N. Bentley,³ Frances A. Staples,¹ Quanqi Shi⁴

¹Mullard Space Science Lab, UCL, UK

²University of Maryland, USA

³University of Reading, UK

⁴Shandong University, China

Corresponding author: Jonathan Rae (jonathan.rae@ucl.ac.uk)

Key Points:

- We determine the Alfvén continuum and enhancement of global Ultra-Low Frequency (ULF) waves during the 2013 St. Patrick's Day geomagnetic storm
- When the Alfvén continuum plummets, lower frequency waves are able to penetrate far deeper into the magnetosphere than expected
- Both solar wind and internal geomagnetic conditions must be considered for the penetration of ULF waves into the inner magnetosphere.

Abstract

Wave-particle interactions play a key role in radiation belt dynamics. Traditionally, Ultra-Low Frequency (ULF) wave-particle interaction is parameterised statistically by a small number of controlling factors for given solar wind driving conditions or geomagnetic activity levels. Here, we investigate solar wind driving of ultra-low frequency (ULF) wave power and the role of the magnetosphere in screening that power from penetrating deep into the inner magnetosphere. We demonstrate that, during enhanced ring current intensity, the Alfvén continuum plummets, allowing lower frequency waves to penetrate deeper into the magnetosphere than during quiet periods. With this penetration, ULF wave power is able to accumulate closer to the Earth than characterised by statistical models. During periods of enhanced solar wind driving such as coronal mass ejection driven storms, where ring current intensities maximise, the observed penetration provides a simple physics-based reason for why storm-time ULF wave power is different compared to non-storm time waves.

Plain Language Summary

Geomagnetic storms are the most dynamic and unpredictable phenomena in near-Earth space. During geomagnetic storms, the Van Allen Radiation Belts can be significantly enhanced, via a number of physical processes. One of these processes is the action of large-scale Ultra-Low Frequency (ULF) waves which are in large part directly related to the prevailing solar wind conditions. In this study, we show that the conditions and internal structuring in near-Earth space during a geomagnetic storm dictate how close to the Earth these large-scale waves can reach. Through a combination of ground-based and in-situ measurements, we show how magnetic field strength and heavy ions control where these waves can access. We show that conditions both internal and external to near-Earth space must be taken into account to understand the behavior of waves, and therefore radiation belt particle dynamics, during geomagnetic storms.

1 Introduction

To provide a physically sound basis for models of energetic, relativistic electron dynamics (with energies >500 keV) in the radiation belts, the balance between acceleration, transport and loss processes must be known. Electromagnetic waves across a large range of frequencies mediate the energy transfer processes in the plasma through a myriad of wave-particle interactions. This is especially true during geomagnetic storms, where the electrons in the radiation belt and the electromagnetic waves shaping their dynamics are at their most variable (Murphy et al., 2016; Watt et al., 2017).

Very Low Frequency (VLF) chorus waves play a fundamental role in radiation belt electron dynamics driving loss to the upper atmosphere (O'Brien et al., 2004) and acceleration within the heart of the outer radiation belt (Reeves et al., 2013). These waves are a critical process for modeling storm-time dynamics of the outer radiation belt (Thorne et al., 2013). Electromagnetic ion cyclotron (EMIC) and VLF hiss waves are largely associated with rapid and slow loss from the radiation belts respectively (Loto'aniu et al., 2006; Thorne et al., 2013). ULF waves transport and energize electrons via discrete resonances (e.g., Mann et al., 2013) and diffusive radial transport (e.g. Falthammer, 1965).

Recent work demonstrated both ULF and VLF waves are highly variable during storms and poorly characterized by empirical wave models (e.g., Ma et al., 2018; Murphy et al., 2016; Tu et al., 2013; Watt et al., 2017). For instance, Tu et al. (2013) have shown that event-specific VLF chorus diffusion coefficients can be two orders of magnitude larger than to those derived from empirical models. Murphy et al. (2016) demonstrated that storm-time ULF wave power is highly variable and can be several orders of magnitude larger than that predicted by empirical wave models.

It is not well understood why differences should exist between storm-time and non storm-time waves. The basic concept of MHD wave propagation in the magnetosphere is that, for a given wave frequency, its penetration is determined by the background magnetic field profile, the mass density and azimuthal wavenumber (Lee, 1996; Figure 4). MHD waves will partially reflect and the wave power will evanesce where the MHD wave mode reaches a turning point (i.e. the cut-off frequency exceeds the wave frequency). The fundamental mode eigenfrequency lies earthward of the turning point. Consequently, the global eigenfrequency configuration is indicative of how deeply ULF wave power of a given frequency and wavenumber can access the inner magnetosphere. Here, we investigate a storm occurring during the Van Allen Probe era, to determine why storm-time ULF wave power may be so different than statistical norms.

2 2013 St Patrick's Day Storm

2.1 General Overview

The 2013 St. Patrick's Day storm forms one of the radiation belt challenge events from the Quantitative Assessment of Radiation Belt Modeling focus group of the Geospace Environment Modeling (GEM) program (<http://bit.ly/28UnLpw>) that has already been remarkably well studied in the literature (e.g., Albert et al., 2018; Engebretson et al., 2018; Ma et al., 2018). Figure S1

shows an overview of the solar wind and magnetospheric observations from 15-21 March 2013 inclusive and the overview of the event.

2.2 Background Alfvén Continuum

ULF waves generated at the magnetopause as a result of the interaction of the Earth's magnetosphere with the solar wind are reflected and refracted as they approach the inner magnetosphere by the Alfvén continuum (e.g., Mathie et al., 1999). The Alfvén continuum determines how deep fast mode waves with a specific frequency may propagate into the magnetosphere from the magnetopause. ULF waves generated at the magnetopause propagate radially inwards without generally losing energy. The Alfvén continuum determines the location at which the fast mode would enter the evanescent regime, and at which point the fast mode can couple to the Alfvén mode and drive toroidal-mode field line resonances (FLRs) (Samson et al., 1971).

It is difficult to determine the global Alfvén continuum from space-based measurements, however this is routinely possible for the dayside hemisphere from ground-based magnetometer measurements (e.g., Waters et al., 1991). Cross-phase analysis can determine the fundamental resonant eigenfrequency between two magnetometer stations (Supplementary material S2) and we use the CARISMA (Canadian Array for Realtime Investigations of Magnetic Activity; Mann et al., 2008) array, using the technique documented by Sandhu et al. [2018a].

Figure 1 shows the results of this automated cross-phase analysis. Each panel displays the median field line eigenfrequency as a function of L-shell, separated into dawn sector (0600-1200 MLT, solid lines) and dusk sectors (1200-1800 MLT, dashed lines) for each of the days of 15-21 March 2013 inclusive.

Field line eigenfrequencies are dependent upon the length of, and Alfvén velocity along, a given field line. During normal conditions, the eigenfrequency decreases monotonically with radial distance in regions inside and outside the plasmapause because the dominant magnetic field strength decays and field line lengths increase. Across the plasmapause, the plasma density drops sharply with radial distance, and the eigenfrequency will increase with radial distance over a short span of L (see Figure F1, Kale et al., 2007).

On 15 March 2013, the Alfvén eigenfrequency continuum displays the same behavior described above, with a small plasmapause reversal between $L = 4.2 - 4.3$ in the dusk sector. During 16 March 2013, the eigenfrequency profile is highly variable, at increased or similar frequencies across all L-shells in the dawn sector. In the dusk sector, eigenfrequencies decrease slightly at low-L and increase sharply at $L \sim 5$, which may indicate the presence of a plasmaspheric plume.

On 17 March 2013, however, there is little evidence of any increasing plasmapause gradient in the continuum across all L and the eigenfrequencies have reduced across all L-shells outside $L = 3.4$. There is some evidence of an MLT asymmetry; that dawn eigenfrequencies are higher than those at dusk. This reduction in the Alfvén continuum is concurrent with the arrival of the CME and the initiation of this geomagnetic storm around 0500 UT.

On 18 March 2013, there are still some dawn-dusk differences in eigenfrequency profiles inside of $L = 4.2$, whereby dawn frequencies are up to 50% higher than their dusk counterparts. All

eigenfrequencies inside of $L \sim 5$ are also higher than their counterparts on the previous day. Both increases in eigenfrequencies and asymmetries in the plasmaspheric density are consistent with the presence of the remnants of a plasmaspheric density plume of the previous day (e.g., Borovsky and Denton, 2008).

On 19 March 2013, the eigenfrequency profiles return to similar values as 17 March 2013, and the differences between the dawn and dusk asymmetries have reduced. Towards the end of the period examined, on 20 and 21 March 2013, significant MLT and L-shell variations are found. The eigenfrequency profiles are very different in each MLT sector, and the eigenfrequency values at around $L=5$ are much larger than they were on 19 March 2013. These major changes are coincident with the arrival of the secondary CME (see previous section) at around 1200 on 20 March 2013. We discuss these changes in the eigenfrequency profile in terms of plasma density evolution through the two consecutive geomagnetic storms.

2.3 Storm-time ULF wave power

We take the vector summed power from the CARISMA (Mann et al., 2008) and IMAGE (Lühr, 1994) magnetometer networks throughout the storm across 51 magnetometers in the same manner as Murphy et al. (2015; 2016) and Mann et al. (2015) and limit our analysis to the dayside hemisphere only and compare this with Figure 1. We limit the analysis to the dayside such that the powers are not influenced by substorm activity (Murphy et al., 2011; Rae et al., 2011).

We use 51 magnetometers to calculate the summed ULF power between 0.83-15.83 mHz at 1 hour resolution throughout the storm period and interpolated onto a uniform 2D grid (original data - Supplementary Material S3).

Figure 2 (top) shows the results of this ground-based analysis of summed ULF wave power as a function of L and time from 15-22 March 2013. Clear from Figure 2 (top) is that the ULF wave activity is highly time-dependent during the period of interest. The ULF wave power across the storm varies both in strength and in penetration depth into the magnetosphere and across multiple frequencies (see Supplementary Material S4).

There are also interesting ULF wave signatures at other times that can be associated with other solar wind drivers. Two enhancements in ULF wave power across all L are seen early on 15 March 2013 and the morning of 16 March 2013. Using the statistical results of Bentley et al. (2018) as an aid, the ULF wave power enhancements on the morning of 15 March 2013 are likely related to the large change in plasma density and negative IMF B_z seen in the solar wind. A similar negative IMF B_z deflection accompanied by a smaller change in plasma density are also seen on the morning of 16 March 2013. Prior to the CME arrival (17 March 2013), the ULF wave activity was quiet and significant ULF wave power ($10 \text{ nT}^2/\text{mHz}$) was not seen any further inside the magnetosphere than $L \sim 6$. However, on arrival of the CME, the ULF waves are enhanced across all L -shells, the power increasing to $>10^3 \text{ nT}^2/\text{mHz}$ at high L , and reaching $10^2 \text{ nT}^2/\text{mHz}$ at $L=3$. The increase in ULF wave activity at high L is likely associated with the significant increase in solar wind velocity and negative IMF B_z that accompany the start of the CME, but what is most interesting is just how far inside the magnetosphere the increase in ULF wave power is seen.

In the ensuing recovery phase on 18 March 2013, the ULF wave power reduces in strength across all locations. Interestingly, the wave amplitude at high L is fairly constant throughout 18 March and into the morning of 19 March 2013. However, the wave activity increases abruptly at lower L in the early hours of 19 March 2013 before decreasing again to a background level a few hours later.

Finally, on the morning of the 21 March 2013, ULF wave power is once again enhanced, reaching $103 \text{ nT}^2/\text{mHz}$ at high L, and $>101 \text{ nT}^2/\text{mHz}$ at $L=3$, presumably due to the arrival of the second CME with its increase in solar wind velocity and subsequent ULF energization. We discuss the role of external driving and internal background Alfvén continuum in this energization below.

Figure 2 (bottom) shows a 2D interpolation of the results shown in Figure 1 of the Alfvén continuum as a function of L-shell and time where colour indicates frequency. A similar type of interpolation has been performed as in the top panel, with a 6 hour time scale, and 0.5 L spatial scale. Overplotted on Figure 2 (bottom) are isocontours of specific frequencies (5, 7 and 9 mHz) to highlight the variability of the location of a particular eigenfrequency over the course of the interval.

Figure 2 (bottom) shows that there is significant structuring of the Alfvén continuum as a function of L and time. Specifically, if we consider the propagation of ULF waves inwards through the magnetosphere, then the continuum structure prior to the storm (i.e. on 15 and 16 March 2013) would enable ULF wave energy at high frequencies ($>10\text{mHz}$) to access the inner magnetosphere, but frequencies lower than that would be reflected and refracted or evanesce. However, once the storm main phase has commenced, the eigenfrequency profile reduces dramatically, such that wave frequencies of 5 mHz could propagate into the inner magnetosphere without hindrance. The 9 mHz contour moves in to $L<3.5$ after the storm modifies the magnetosphere, as compared to the period prior to the storm where the 9 mHz contour exists at $L>5$. Figure S4 shows ULF wave power at these specific frequencies of 5, ~ 7 and ~ 9 mHz, and demonstrates that the ULF wave power at given frequencies does indeed penetrate to lower-L when the eigenfrequency continuum is suppressed.

As the storm moves into the recovery phase, the ULF wave power in Figure 2 (top) wanes at higher L-shells, at the same time as the Alfvén continuum relaxes, such that 5 mHz contours are now around $L=6$. On 19 March 2013, the Alfvén continuum again reduces to a storm-like level, and we observe another ULF wave penetration event (Figure 2 (top)). Finally, Figure 2 (bottom) shows that towards the end of the interval, at the same time as the second, smaller storm, the pattern of the eigenfrequency continuum is reversed such that low frequencies are observed at low L and vice versa. We conclude that either the plasmopause is around $L\sim 4$ and the eigenfrequency continuum returns to a more typical profile (c.f., Figure 1, Kale et al., 2007) or that there may be a complicated Alfvén continuum due to the recovery phase of one storm coinciding with another.

3 Discussion and Conclusions

ULF waves are a key component of any storm-time study of relativistic electron dynamics, whether they are responsible for direct energization (Claudpierre et al., 2013), transport (Mann et

al., 2015; Ozeke et al, 2018), or losses (e.g., Rae et al., 2018). Here, we investigate the role of ULF waves during a geomagnetically active period, with the critical addition of using the eigenfrequency continuum to monitor the changes in the internal environment of the magnetosphere, as seen by the ULF waves.

It is now established that the main source of global-scale ULF wave power is the solar wind. Global-scale ULF waves have low azimuthal wavenumbers, m , the value of which describes the number of wavelengths around the Earth at a given radial distance. Solar wind speed (Mathie and Mann, 2001; Murphy et al., 2011; Rae et al., 2012) and dynamic pressure (Kepko et al., 2002; Sibeck et al., 1989) have both been studied as controlling factors. However, the interdependence of solar wind parameters can often mask the underlying factors that result in enhanced ULF wave power, necessitating a systematic statistical study. Recently, the relative contributions of solar wind drivers of ULF wave power have been quantified by Bentley et al. (2018). In this work, Bentley et al. (2018) found that solar wind speed was the dominant driver, followed by the southward component of IMF B_z and, in contrast to previous work, the variance in number density, as opposed to the derived dynamic pressure. Statistically, as solar wind driving enhances, ULF wave power increases monotonically at all radial distances in the inner magnetosphere (e.g., Georgiou et al., 2018; Mathie et al., 1999; Rae et al., 2012). However, none of these previous statistical studies take into account the time history of the solar wind, including the temporal behavior of CMEs, corotating interaction regions (CIRs) or other solar wind transients. Hence, the time-dependent nature of the solar wind may be a critical missing factor in empirical models of solar wind driven ULF wave activity.

Equally, the internal plasma conditions of the magnetosphere are typically not considered in parameterized models of ULF wave power. Such models often use a geomagnetic index as a proxy for the external solar wind driving and internal magnetospheric dynamics (e.g. the Kp model of Ozeke et al., (2014)). Physically, ULF wave activity in the magnetosphere is dictated by the background magnetic field strength and the number density and composition of the cold plasma. It is these parameters that control the Alfvén eigenfrequency profile and hence the accessibility of ULF wave power into a given magnetospheric location.

Figure 1 shows the variation of the Alfvén continuum with L-shell, frequency and time throughout the 2013 St. Patrick’s Day storm. During the storm main phase, the Alfvén continuum is suppressed at the vast majority of L-shells, other than around $L=3.4$ where there is some evidence of a newly formed or refilling plasmopause. The consequence of this is that prior to the storm, only frequencies greater than 12 mHz could access the inner magnetosphere without evanescently decaying. During the main phase of the storm, suddenly any frequencies greater than 5 mHz can now penetrate into the inner magnetosphere as deep as $L=3.4$.

During this storm, the ULF wave power (Figure 2 (top)) is highly dynamic, varying by 3 orders of magnitude. Storm-time ULF wave power has been shown to be significantly variable during the main phase of the storm (e.g., Loto’aniu et al., 2006; Murphy et al., 2016). During one of the largest geomagnetic storms in recent history, the “Halloween storm” of 2003, Loto’aniu et al. (2006) found that ULF wave power varied by 4 orders of magnitude. Interestingly these authors also found that ULF wave power was most enhanced during the two storm main phases. More specifically, the largest ULF wave power during the Halloween storm occurred during the three periods of increasingly negative Dst index.

During periods where the eigenfrequencies are lower, ULF wave power reaches deeper into the magnetosphere (Figure 2). ULF wave power inside the magnetosphere has a power law like power spectrum (Bentley et al., 2018; Rae et al., 2012). Hence, when lower frequencies can access lower L-shells, the summed ULF wave power is generally higher. When the Alfvén profile recovers between 19-20 March 2013, ULF wave power is screened from the inner magnetosphere. However, when the second geomagnetic storm occurs on the 20 March 2013, ULF wave power again accesses the inner magnetosphere. By inspection of Figure 1 and Figure 2, it is clear that the eigenfrequency variations are complex, but this may result in plasmaspheric plumes significantly complicating the simple ULF wave dynamics that are described in the current literature. Essentially, when there are both radial and azimuthal gradients in the Alfvén continuum, there is a frequency dependent accumulation and penetration of ULF wave power through, and indeed within, the plume (c.f., Figure 3(a), Degeling et al., 2018), which will complicate the magnetospheric location of ULF wave powers.

The natural eigenfrequency of geomagnetic field lines is determined by its magnetic field profile and the mass density along the field line. During geomagnetic storms, it is usually thought that heavy ion outflow increases the mass density sufficiently to lower the Alfvén continuum (e.g., Engwall et al. 2009; Kale et al., 2009; Kronberg et al., 2014; Loto'aniu et al., 2006; Yau et al., 1988). Certainly heavy ions must play a role. However, Sandhu et al (2018b) constructed a statistical model of the average mass densities as a function of Dst index. Sandhu et al. (2018b) found that, although the average ion mass did increase significantly with increasingly negative Dst index, the electron densities in the inner magnetosphere reduced.

Hence on average, lower Dst index values reduce the plasma mass density, rather than increasing it as previously thought. Sandhu et al. (2018b) concluded that the changes in the magnetic field drove the changes in eigenfrequency; during sudden increases in dayside compression, the geomagnetic field strength in the outer magnetosphere increases across the dayside. It is important to remember that when using a proxy such as Dst index, two very different intervals are averaged, decreasing Dst during the main phase and increasing Dst during the recovery phase even though both phases pass through the same values of Dst. However, Sandhu et al's (2018b) model provides useful context for interpreting our results. We now consider the role of the ring current itself in reducing the Alfvén continuum in the inner magnetosphere. Commonly, the "Dst effect" (Kim and Chan, 1997) is specifically limited to the effect of ring current enhancement encouraging electron loss. Here we suggest that the strengthening ring current significantly changes the Alfvén continuum during key periods of the storm.

Relationships between ring current intensity and ULF wave power have been discussed previously (e.g., Mann et al., 2012; Murphy et al, 2014), suggesting a causal link between ring current ions and the generation of storm-time high-m waves that could play additional roles in energization (eg., Ozeke and Mann, 2008) and loss (e.g., Rae et al., 2018). Clearly, it is the interplay between magnetic field and plasma mass densities that is key during the dynamic period in main phase of the storm. Figures 2 and 3 (bottom) show that the eigenfrequencies are suppressed during this storm main phase.

In order to reduce the Alfvén continuum across a wide range of L-shells, the magnetic field strength must reduce, or the mass density must increase, or a combination of both. Figure 3(a) demonstrates the effect of the ring current in reducing the local magnetic field strength at the

Van Allen Probes A and B throughout the storm, by displaying the ratio between the magnetic field strength observed by Van Allen Probes (Kletzing et al., 2014) relative to the IGRF (International Geomagnetic Reference Field). Note that there is a clear reduction in the ratio away from 1.0 in the same manner as Shen et al. (2014) discussed that is mirrored by the negative enhancement in the Dst index. This implies that the expected magnetic field as measured by the Van Allen Probes is significantly suppressed during the storm main phase and in response to the evolving ring current.

There are a number of factors at play here, however. Field line eigenfrequencies are influenced by the magnetic field strength and by plasma mass density along the field. In this paper, we discuss how the inner magnetosphere could respond differently to geomagnetic storms than the outer magnetosphere. Ion outflow during geomagnetic storms (e.g., Yau et al., 1988) would certainly influence the plasma mass density at all locations during the main phase of the storm. However, there is also a secondary effect, which is that there is also enhanced helium and oxygen ring current ions in the inner magnetosphere (e.g., Sandhu et al., 2018c). The enhanced ring current (and its contribution to mass densities) will increase the heavy ion content in the inner magnetosphere, whilst also reducing the local magnetic field strength at ring current radial distances (Kim and Chan, 1997; Kronberg et al., 2014). Regardless of which effect is dominant, these additive effects lead to a net decrease in the Alfvén continuum, allowing deep penetration of ULF wave power into the inner magnetosphere during periods of increase ring current intensity. It must be stressed that the amplitude of this ULF wave accessibility is dependent upon the solar wind driver and, while penetration can occur during ring current enhancements, large amplitude wave power at low-L will occur during periods of enhanced solar wind driving and ring current intensities (e.g., Loto'aniu et al., 2006). The plasmopause role on Pc5 penetration has been reported before by Hartinger et al. [2010]. Here, we discuss that multiple storm-time factors of plasma composition and density, global magnetic field configuration and the suppression of the inner magnetospheric field by the ring current can depress the Alfvén continuum.

Figure 3(b-e) shows ion data from the Van Allen Probes HOPE (Helium Oxygen Proton Electron) instruments (Funsten et al., 2013; Spence et al., 2013) during the storm. Figure 3(b-e) shows (b) H⁺, (c) O⁺ energy fluxes as a function of energy and time, and (d) the ratio between these fluxes. Figure 3(c) shows the increase in both low energy oxygen (<100 eV) on 17 March 2013 at ~12 UT, and the delayed increase of higher energy oxygen (100eV-100keV) later in the geomagnetic storm from 12 UT on 18 March 2013, and with a slow decay lasting ~1-2 days. This two-step heavy ion increase is consistent with the sharp increase in ion outflow at the start of the geomagnetic storm (e.g., Gkioulidou et al., 2019; Kronberg et al., 2014) and the longer-term penetration of heavy ions convected into the inner magnetosphere from substorms (e.g., Sandhu et al., 2018). Figure 3(d) shows the ratio of oxygen to hydrogen as a function of energy, and (e) summed over energy to demonstrate intervals where the heavy ion content of the ring current should be considered to be significant; the dashed horizontal line indicating unity. On 17 March, the increase in low energy oxygen and the decrease in low energy hydrogen leads to a large increase in the ratio. The hydrogen content of the ring current recovers over the course of the 18 March 2013 and there is an additional higher energy oxygen content which maintains an elevated ratio as seen in Figure 3(e). The additive effect of reduced magnetic field and two-step heavy ion content leads to a suppressed Alfvén continuum that is highly variable throughout the entire storm-time period, enabling mHz frequencies to penetrate the inner magnetosphere as a

consequence. We conclude that solar wind driving as well as current internal conditions must both be considered for realistic storm-time ULF wave conditions in the inner magnetosphere.

It is interesting to note that the lowering of the continuum and penetration of ULF wave power is closely coincident with the time and location of rapid enhancement in MeV electron fluxes (Figure S1), as both ULF wave power and enhancements occur around $L=3-3.5$. Such penetration may also explain slot region filling during very large storms, where both ULF wave powers and ring current intensities are largest (Ozeke et al., 2018). What role this ULF wave power plays in shaping the radiation belt enhancement remains to be seen, but what is clear is that ULF wave powers must be taken into account during radiation belt modelling of such enhancements.

One of the primary challenges of the Quantitative Assessment of Radiation Belt Morphology (QARBM) Geospace Environment Modeling (GEM) challenge is to assess the validity of diffusion coefficients during specific geomagnetic storms. Since the accessibility of ULF wave power is strongly dependent upon internal geomagnetic conditions, we conclude that the radial dependence of ULF wave diffusion coefficients will vary significantly during geomagnetic storms not only on external driving but also critically on internal factors that have not yet been fully considered.

Acknowledgments

This research was supported by the Natural Environment Research Council (NERC) Highlight Topic Grant Rad-Sat, and grant numbers NE/P017185/1 and NE/P017274/1, STFC grants ST/N0007722/1 and ST/R000921/1. C.F. is supported by a NERC IRF NE/N014480/1.

All data publically available via www.carisma.ca, <http://space.fmi.fi/image/www/index.php?>, <http://cdaweb.gsfc.nasa.gov> and <http://rbspgway.jhuapl.edu/psd>

References

- Albert, J. M., Selesnick, R. S., Morley, S. K., Henderson, M. G., & Kellerman, A. C. (2018). Calculation of last closed drift shells for the 2013 GEM radiation belt challenge events. *Journal of Geophysical Research: Space Physics*, 123, 9597–9611. <https://doi.org/10.1029/2018JA025991>
- Bentley, S. N., Watt, C. E. J., Owens, M. J. and Rae, I. J. (2018) ULF wave activity in the magnetosphere: resolving solar wind interdependencies to identify driving mechanisms. *Journal of Geophysical Research: Space Physics*, 123 (4). pp. 2745-2771. ISSN 2169-9402 doi: 10.1002/2017ja024740
- Berube, D., M. B. Moldwin, and J. M. Weygand (2003), An automated method for the detection of field line resonance frequencies using ground magnetometer techniques, *J. Geophys. Res.*, 108, 1348, doi:10.1029/2002JA009737, A9.
- Blake, J.B., Carranza, P.A., Claudepierre, S.G. et al. *Space Sci Rev* (2013) 179: 383. <https://doi.org/10.1007/s11214-013-9991-8> Claudepierre, S. G., et al. (2013), Van Allen Probes observation of localized drift resonance between poloidal mode ultra-low frequency waves and 60 keV electrons, *Geophys. Res. Lett.*, 40, 4491–4497, doi:10.1002/grl.50901.
- Degeling, A. W., Rae, I. J., Watt, C. E. J., Shi, Q. Q., Rankin, R., & Zong, Q. -. G. (2018). Control of ULF Wave Accessibility to the Inner Magnetosphere by the Convection of Plasma Density. *JOURNAL OF GEOPHYSICAL RESEARCH-SPACE PHYSICS*, 123 (2), 1086-1099. doi:10.1002/2017JA024874
- Engebretson, M. J., Posch, J. L., Braun, D. J., Li, W., Ma, Q., Kellerman, A. C., et al. (2018). EMIC wave events during the four GEM QARBM challenge intervals. *Journal of Geophysical Research: Space Physics*, 123, 6394–6423. <https://doi.org/10.1029/2018JA025505>
- Engwall, E., A. I. Eriksson, C. M. Cully, M. Andr e, R. Torbert, and H. Vaith (2009), Earth’s ionospheric outflow dominated by hidden cold plasma, *Nature Geoscience*, pp. 24–27, doi: 10.1038/NGEO387
- F lthammar, C.-G. (1965), Effects of time-dependent electric fields on geomagnetically trapped radiation, *J. Geophys. Res.*, 70(11), 2503–2516, doi:10.1029/JZ070i011p02503.
- Funsten, H. O., R. M. Skoug, A. A. Guthrie, E. A. MacDonald, J. R. Baldonado, R. H. Harper, K. C. Henderson, K. H. Kihara, J. E. Lake, B. A. Larsen, A. D. Puckett, V. J. Vigil, R. H. W. Friedel, M. G. Henderson, J. T. Niehof, G. D. Reeves, and M. F. Thomsen (2013), Helium, Oxygen, Proton, and Electron (HOPE) Mass Spectrometer for the Radiation Belt Storm Probes Mission, *Space Science Reviews*, doi:10.1007/s11214-013-9968-7.
- Georgiou, M., I.A. Daglis, I.J. Rae, E. Zesta, D.G. Sibeck, I.R. Mann, G. Balasis, K. Tsinganos (2018), Ultra-low frequency waves as an intermediary for solar wind energy input into the radiation belts, *J. Geophys. Res.*, 123(12), 10,090–10,108

- Gkioulidou, M., Ohtani, S., Ukhorskiy, A. Y., Mitchell, D. G., Takahashi, K., Spence, H. E., et al (2019). Low-energy (<keV) O⁺ ion outflow directly into the inner magnetosphere: Van Allen Probes observations. *Journal of Geophysical Research: Space Physics*, 124, 405–419. <https://doi.org/10.1029/2018JA025862>
- Harteringer, M., Moldwin, M. B., Angelopoulos, V., Takahashi, K., Singer, H. J., Anderson, R. R., Nishimura, Y., and Wygant, J. R. (2010), Pc5 wave power in the quiet-time plasmasphere and trough: CRRES observations, *Geophys. Res. Lett.*, 37, L07107, doi:10.1029/2010GL042475.
- Kale, Z.C., I.R. Mann, C.L. Waters, J. Goldstein, F.W. Menk, and L.G. Ozeke (2007), Ground magnetometer observation of a cross-phase reversal at a steep plasmopause, *J. Geophys. Res.*, 112, A10222, 2007, DOI: 10.1029/2007JA012367.
- Kale, Z. C., I. R. Mann, C. L. Waters, M. Vellante, T. L. Zhang, and F. Honary (2009), Plasmaspheric dynamics resulting from the Halloween 2003 geomagnetic storms, *J. Geophys. Res.*, 114, A08204, doi:10.1029/2009JA014194.
- Kepko, L., H. E. Spence and H. J. Singer (2002), ULF waves in the solar wind as direct drivers of magnetospheric pulsations, *Geophysical Research Letters*, 29, 1197, doi:10.1029/2001GL014405
- Kronberg, Elena A., Maha Ashour-Abdalla, Iannis Dandouras, Dominique C. Delcourt, Elena E. Grigorenko, Lynn M. Kistler, Ilya V. Kuzichev, Jing Liao, Romain Maggiolo, Helmi V. Malova, Ksenia G. Orlova, Vahe Perroomian, David R. Shklyar, Yuri Y. Shprits, Daniel T. Welling, Lev M. Zelenyi (2014), Circulation of Heavy Ions and Their Dynamical Effects in the Magnetosphere: Recent Observations and Models, *Space Science Reviews*, Volume 184, Number 1-4, Page 173
- Lee, D.-H. (1996), Dynamics of MHD wave propagation in the low-latitude magnetosphere, *J. Geophys. Res.*, 101(A7), 15371– 15386, doi:10.1029/96JA00608.
- Loto'aniu, T. M., R. M. Thorne, B. J. Fraser, and D. Summers (2006), Estimating relativistic electron pitch angle scattering rates using properties of the electromagnetic ion cyclotron wave spectrum, *J. Geophys. Res.*, 111, A04220, doi:10.1029/2005JA011452.
- Loto'aniu, T. M., Mann, I. R., Ozeke, L. G., Chan, A. A., Dent, Z. C., & Milling, D. K. (2006). Radial diffusion of relativistic electrons into the radiation belt slot region during the 2003 Halloween geomagnetic storms. *Journal of Geophysical Research*, 111, A04218. doi: 10.1029/2005JA011355
- Lühr, H. (1994). The IMAGE magnetometer network, STEP International (vol. 4, pp. 4–6). USSCO.
- Kim, H.-J., and A. A. Chan (1997), Fully adiabatic changes in storm time relativistic electron fluxes, *J. Geophys. Res.*, 102, 22,107–22,116, doi:10.1029/97JA01814.

- Kletzing, C.A., Kurth, W.S., Acuna, M. et al. (2013), The Electric and Magnetic Field Instrument Suite and Integrated Science (EMFISIS) on RBSP, *Space Sci Rev.*, v. 179, issue 1-4, 127-181.
- Ma, Q., Li, W., Bortnik, J., Thorne, R. M., Chu, X., Ozeke, L. G., Reeves, G. D., et al. (2018). Quantitative Evaluation of Radial Diffusion and Local Acceleration Processes During GEM Challenge Events. *Journal of Geophysical Research (Space Physics)* , 123, 1938-1952.
- Mann, I. R., Milling, D. K., Rae, I. J., Ozeke, L. G., Kale, A., Kale, Z. C., . . . Singer, H. J. (2008). The upgraded CARISMA magnetometer array in the THEMIS era. *Space Science Reviews*, 141 (1-4), 413-451. doi:10.1007/s11214-008-9457-6#
- Mann, I. R., Lee, E. A., Claudepierre, S. G., Fennell, J. F., Degeling, A., Rae, I. J., . . . Honary, F. (2013). Discovery of the action of a geophysical synchrotron in the Earth's Van Allen radiation belts. *Nature Communications*, 4 (1). doi:10.1038/ncomms3795
- Mann, I. R., Murphy, K. R., Ozeke, L. G., Rae, I. J., Milling, D. K., Kale, A., & Honary, F. (2012). The role of ultralow frequency waves in radiation belt dynamics. In D. Summers, I. R. Mann, D. N. Baker, M. Schultz (Eds.), *Dynamics of the Earth's Radiation Belts and Inner Magnetosphere* (pp. 69-91). Washington, D.C.: AGU. doi:10.1029/2012GM001349
- Mann, I. R., Ozeke, L. G., Murphy, K. R., Claudepierre, S. G., Turner, D. L., Baker, D. N., et al. (2016). Explaining the dynamics of the ultra-relativistic third Van Allen radiation belt. *Nature Physics*, 12(10), 978–983. <https://doi.org/10.1038/nphys3799>
- Mathie, R. A., and I. R. Mann (2001), On the solar wind control of Pc5 ULF pulsation power at mid-latitudes: Implications for MeV electron acceleration in the outer radiation belt, *J. Geophys. Res.*, 106(A12), 29783–29796, doi:10.1029/2001JA000002.
- R. A. Mathie F. W. Menk I. R. Mann D. Orr (1999), Discrete Field Line Resonances and the Alfvén Continuum in the Outer Magnetosphere, *Geophys. Res. Lett.*, doi: 10.1029/1999GL900104
- Frederick Menk, Zoë Kale, Murray Sciffer, Peter Robinson, Colin Waters, Russell Grew, Mark Clilverd, Ian Mann (2014), Remote sensing the plasmasphere, plasmopause, plumes and other features using ground-based magnetometers, *J. Space Weather Space Clim.* 4 A34, DOI:10.1051/swsc/2014030
- Murphy, K. R., Rae, I. J., Mann, I. R., & Milling, D. K. (2011). On the nature of ULF wave power during nightside auroral activations and substorms: 1. Spatial distribution. *Journal of Geophysical Research: Space Physics*, 116 (1). doi:10.1029/2010JA015757
- Murphy, K. R., I. R. Mann, and L. G. Ozeke (2014), A ULF wave driver of ring current energization, *Geophys. Res. Lett.*, 41, 6595–6602, doi:10.1002/2014GL061253.
- Murphy, K. R., Mann, I. R., & Sibeck, D. G. (2015). On the dependence of storm time ULF wave power on magnetopause location: Impacts for ULF wave radial diffusion. *Geophysical Research Letters*, 42, 9676–9684. <https://doi.org/10.1002/2015GL066592>

- Murphy, K. R., Mann, I. R., Rae, I. J., Sibeck, D. G., & Watt, C. E. J. (2016). Accurately characterizing the importance of wave-particle interactions in radiation belt dynamics: The pitfalls of statistical wave representations. *Journal of Geophysical Research: Space Physics*, 121 (8), 7895-7899. doi:10.1002/2016JA022618
- O'Brien, T. P., M. D. Looper, and J. B. Blake (2004), Quantification of relativistic electron microburst losses during the GEM storms, *Geophys. Res. Lett.*, 31, L04802, doi:10.1029/2003GL018621.
- Ozeke, L. G., and I. R. Mann (2008), Energization of radiation belt electrons by ring current ion driven ULF waves, *J. Geophys. Res.*, 113, A02201, doi:10.1029/2007JA012468.
- Ozeke, L. G., Mann, I. R., Murphy, K. R., Rae, I. J., Milling, D. K., Elkington, S. R., . . . Singer, H. J. (2012). ULF wave derived radiation belt radial diffusion coefficients. *Journal of Geophysical Research: Space Physics*, 117 (4). doi:10.1029/2011JA017463
- Ozeke, L. G., I. R. Mann, K. R. Murphy, A. W. Degeling, S. G. Claudepierre and H. E. Spence (2018), Explaining the apparent impenetrable barrier to ultra-relativistic electrons in the outer Van Allen belt, *Nature Comms.* 9, 1844.
- Press, W. (1992). *Numerical recipes in C: The art of scientific computing*, no. bk. 4 in numerical recipes in C : the art of scientific computing. New York, NY, USA: William H. Press, Cambridge University Press.
- Louis G. Ozeke, Ian R. Mann, Kyle R. Murphy, Alex W. Degeling, Seth G. Claudepierre & Harlan E. Spence (2018), Explaining the apparent impenetrable barrier to ultra-relativistic electrons in the outer Van Allen belt, *Nature Communications*, volume 9, Article number: 1844
- Rae, I. J., Mann, I. R., Murphy, K. R., Ozeke, L. G., Milling, D. K., Chan, A. A., . . . Honary, F. (2012). Ground-based magnetometer determination of in situ Pc4-5 ULF electric field wave spectra as a function of solar wind speed. *Journal of Geophysical Research: Space Physics*, 117 (4). doi:10.1029/2011JA017335
- Rae, I. J., Murphy, K. R., Watt, C. E. J., & Mann, I. R. (2011). On the nature of ULF wave power during nightside auroral activations and substorms: 2. Temporal evolution. *Journal of Geophysical Research: Space Physics*, 116 (1). doi:10.1029/2010JA015762
- Rae, I.J., Murphy, K. R., Watt, C. E. J., Halford, A. J., Mann, I. R., Ozeke, L. G., Sibeck, D. G., Clilverd, M. A., Rodger, C. J., Degeling, A. W., Forsyth, C. and Singer, H. J. (2018) The role of localised compressional Ultra-Low Frequency waves in energetic electron precipitation. *Journal of Geophysical Research: Space Physics*, 123 (3). pp. 1900-1914. ISSN 2169-9402 doi: 10.1002/2017ja024674
- G.D. Reeves, H.E. Spence, M.G. Henderson, R.H.W. Friedel, H.O. Funsten, D.N. Baker, S.G. Kanekal, J.B. Blake, J.F. Fennell, S.G. Claudepierre, R.M. Thorne, D.L. Turner, C.A. Kletzing, W.S. Kurth, B.A. Larsen, J.T. Niehof, S.K. Morley (2013), Electron acceleration in the heart of the Van Allen radiation belts, *Science*, 341(6149):991-4. doi: 10.1126/science.1237743

- 508 Sandhu, J. K., Yeoman, T. K., James, M. K., Rae, I. J., & Fear, R. C. (2018a). Variations of
509 high-latitude geomagnetic pulsation frequencies: A comparison of time-of-flight estimates and
510 IMAGE magnetometer observations. *Journal of Geophysical Research: Space Physics*, 123, 567–
511 586. <https://doi.org/10.1002/2017JA024434>
- 512 Sandhu, J. K., Yeoman, T. K., & Rae, I. J. (2018b). Variations of Field Line Eigenfrequencies
513 With Ring Current Intensity. *Journal of Geophysical Research: Space Physics*.
514 doi:10.1029/2018JA025751
- 515 Sandhu, J. K., Rae, I. J., Freeman, M. P., Forsyth, C., Gkioulidou, M., Reeves, G. D., et al.
516 (2018c). Energization of the ring current by substorms. *Journal of Geophysical Research: Space*
517 *Physics*, 123, 8131–8148. <https://doi.org/10.1029/2018JA025766>
- 518 Samson, J. C., J. A. Jacobs, and G. Rostoker, Latitude dependent characteristics of long-period
519 geomagnetic pulsations, *J. Geophys. Res.*, 76, 3675, 1971.
- 520 Shen, C., et al. (2014), Direct calculation of the ring current distribution and magnetic structure
521 seen by Cluster during geomagnetic storms, *J. Geophys. Res. Space Physics*, 119, 2458–2465,
522 doi:10.1002/2013JA019460.
- 523 Shue, J.-H., et al. (1998), Magnetopause location under extreme solar wind conditions, *J.*
524 *Geophys. Res.*, 103(A8), 17691–17700, doi:10.1029/98JA01103.
- 525 Sibeck, D.G., Baumjohann, W., Elphic, R.C., Fairfield, D.H., Fennell, J.F. (1989), The
526 magnetospheric response to 8--minute period strong--amplitude upstream pressure variations, *J.*
527 *Geophys. Res.*, 94(a3),2505–2519
- 528 Spence, H. E., G. D. Reeves, D. N. Baker, J. B. Blake, M. Bolton, S. Bourdarie, A. H. Chan, S.
529 G. Claudpierre, J. H. Clemmons, J. P. Cravens, S. R. Elkington, J. F. Fennell, R. H. W. Friedel,
530 H. O. Funsten, J. Goldstein, J. C. Green, A. Guthrie, M. G. Henderson, R. B. Horne, M. K.
531 Hudson, J.-M. Jahn, V. K. Jordanova, S. G. Kanekal, B. W. Klatt, B. A. Larsen, X. Li, E. A.
532 MacDonald, I. R. Mann, J. Niehof, T. P. O'Brien, T. G. Onsager, D. Salvaggio, R. M. Skoug, S.
533 S. Smith, L. L. Suther, M. F. Thomsen, and R. M. Thorne (2013), Science Goals and Overview
534 of the Energetic Particle, Composition, and Thermal Plasma (ECT) Suite on NASA's Radiation
535 Belt Storm Probes (RBSP) Mission, *Space Science Reviews*, doi:10.1007/s11214-013-0007-5.
- 536 Thorne, R. M., et al. (2013), Evolution and slow decay of an unusual narrow ring of relativistic
537 electrons near $L \sim 3.2$ following the September 2012 magnetic storm, *Geophys. Res. Lett.*, 40,
538 3507–3511, doi:10.1002/grl.50627.
- 539 Tu, W., G. S. Cunningham, Y. Chen, M. G. Henderson, E. Camporeale, and G. D. Reeves
540 (2013), Modeling radiation belt electron dynamics during GEM challenge intervals with the
541 DREAM3D diffusion model, *J. Geophys. Res. Space Physics*, 118, 6197–6211,
542 doi:10.1002/jgra.50560.
- 543 Waters, C. L., F. W. Menk, and B. J. Fraser (1991), The resonance structure of low latitude Pc3
544 geomagnetic pulsations, *Geophys. Res. Lett.*, 18(12), 2293–2296.

- 545 Waters, C. L., J. C. Samson, and E. F. Donovan (1995), The temporal variation of the frequency
546 of high latitude field line resonances, *J. Geophys. Res.*, 100(A5), 7987–7996.
- 547 Watt, C. E. J., Rae, I. J., Murphy, K. R., Anekallu, C., Bentley, S., & Forsyth, C. (2017). The
548 parameterization of wave-particle interactions in the Outer Radiation Belt. *Journal of*
549 *Geophysical Research: Space Physics*. doi:10.1002/2017JA024339
- 550 A.W. Yau, W.K. Peterson, E.G. Shelley (1988), Quantitative parametrization of energetic
551 ionospheric ion outflow, in *Modeling Magnetospheric Plasma*, ed. by T.E. Moore et al..
552 *Geophys. Monogr. Ser.*, vol. 44 (AGU, Washington D.C.), pp. 211–217
553

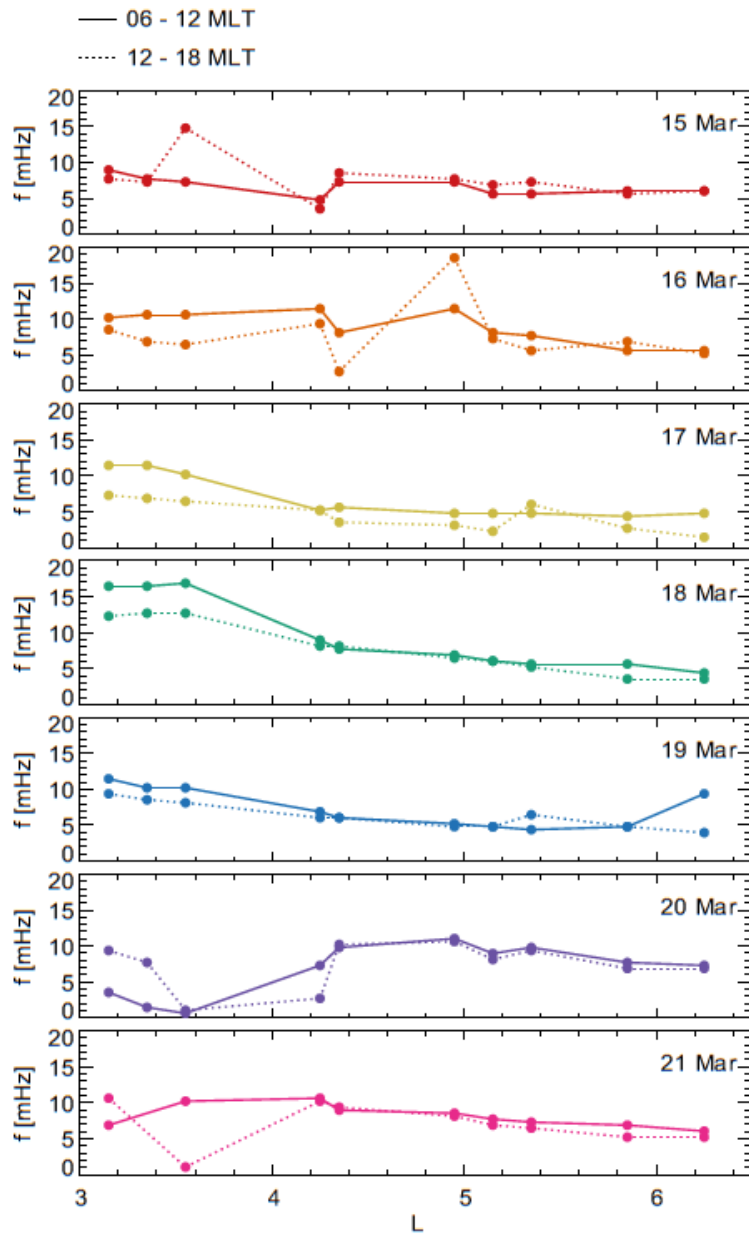


Figure 1. Eigenfrequency profiles from the CARISMA magnetometer array “Churchill Line” (see Supplementary S2). Figure 1 contains the cross-phase results using the automated algorithm from Sandhu et al. [2018a] from measurements from station pairs shown in Supplementary Material S2.

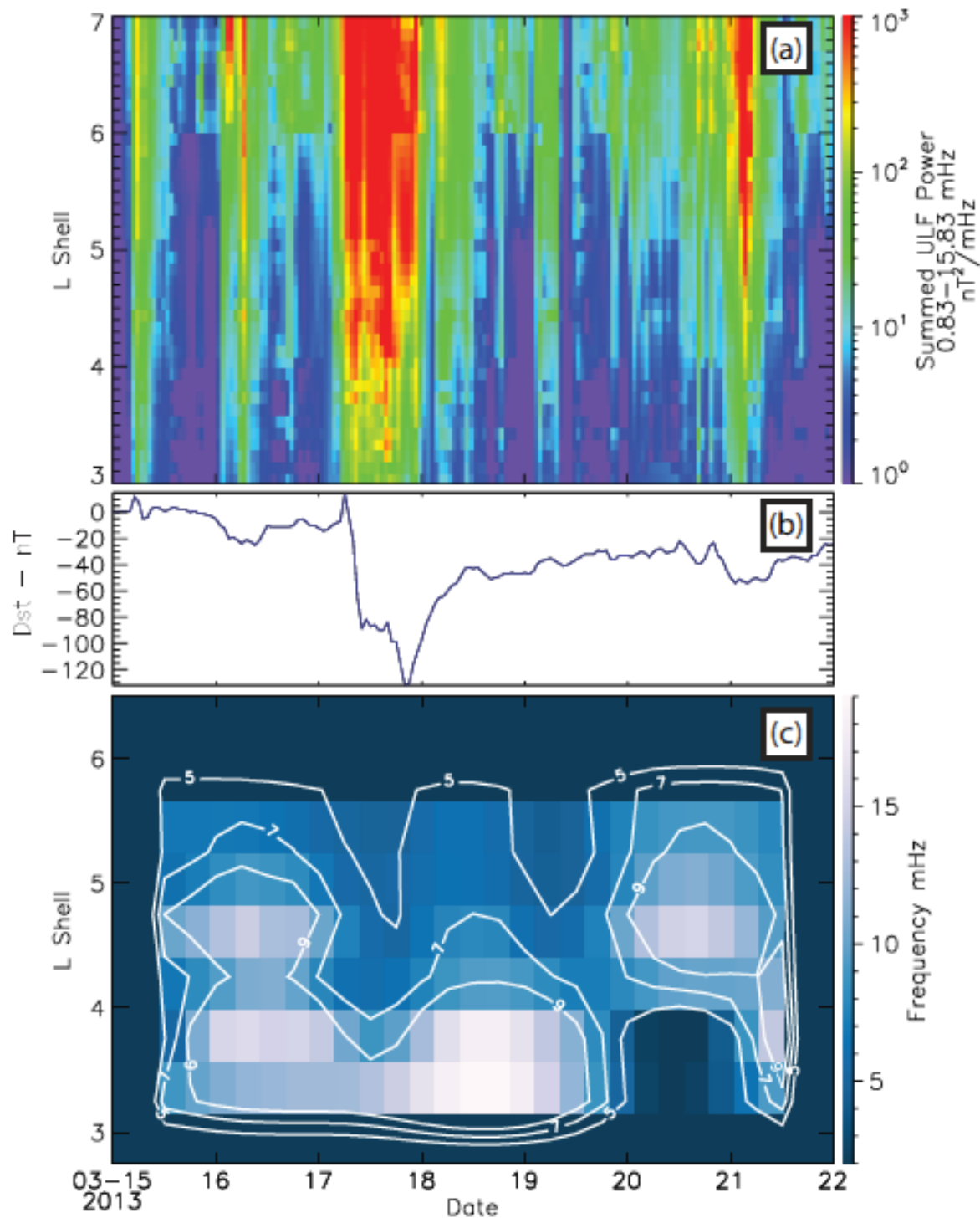


Figure 2. (top) Summed ULF wave power from the IMAGE and CARISMA magnetometer chains for the 15-22 March 2013 storm over the dayside magnetosphere (06-18 MLT) interpolated onto a 2D grid with 1hour resolution and 0.1L step (original data in Supplementary Material S2). (bottom) a 2D interpolation with 6 hours in time and 0.25 L spatial scales of the Alfvén continuum shown in Figure 1.

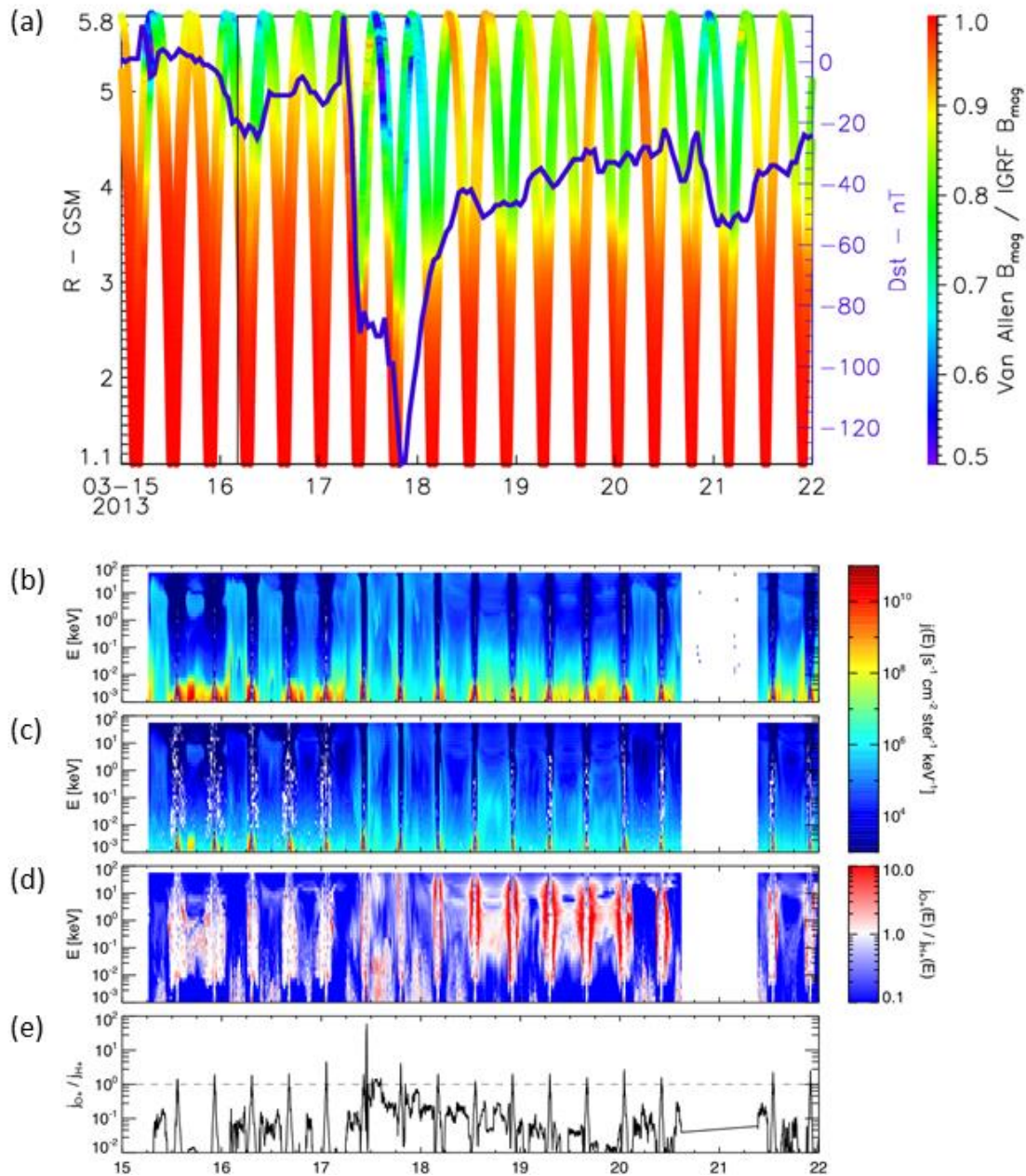


Figure 3. (a) Comparison between observed field magnitude from Van Allen Probes A and B and the International Geomagnetic Reference Field (IGRF) field model. Figure 3(a) shows the ratio of observed magnitude to IGRF magnitude as a function of radial distance and time. Overplotted on the right axis is the Dst index. Figure 3(b-e). HOPE observations of omnidirectional energy flux for H⁺ ions, $jH+(E)$, and O⁺ ions, $jO+(E)$, averaged at 5 minute resolution from 15 - 22 March 2015. Figure 3 (b,c) energy spectrograms of $jH+(E)$ and $jO+(E)$, respectively. (d) energy spectrogram showing the ratio of $jO+(E)$ to $jH+(E)$. (e) the ratio of $jO+(E)$ to $jH+(E)$ summed over all energies shown in Figure 3 (d).

Figure 1.

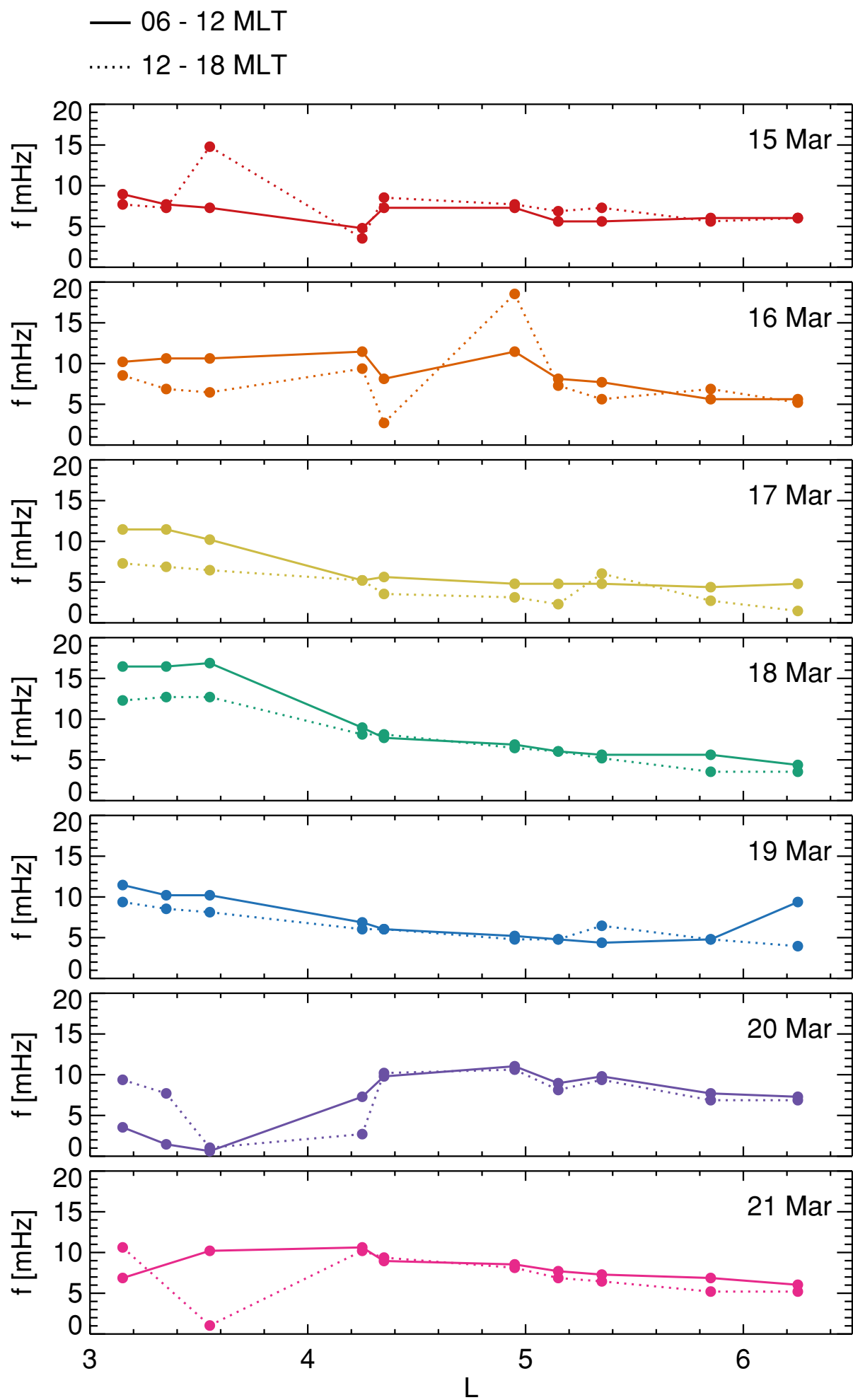


Figure 2.

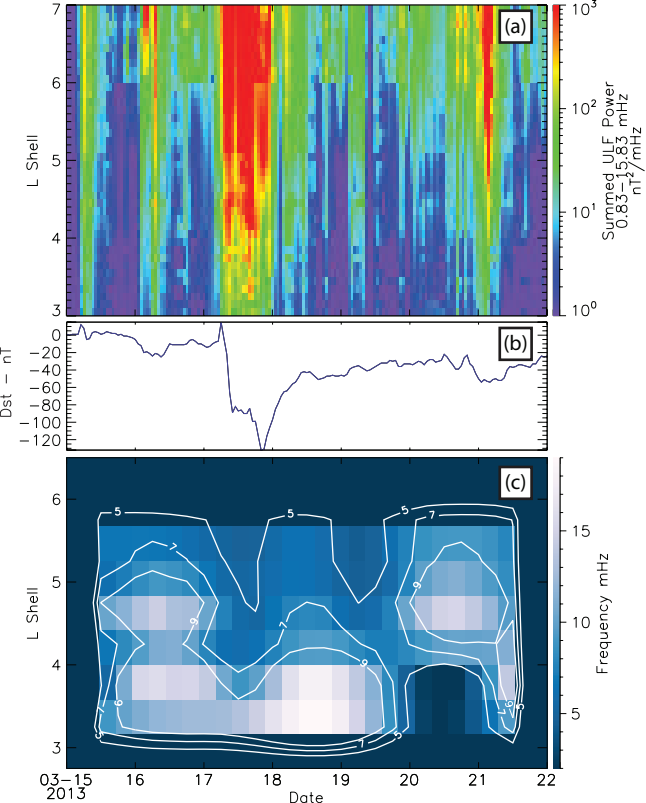


Figure 3.

